Polymer nanocomposites for plasmonics: *In situ* synthesis of gold nanoparticles after additive manufacturing

Wera Di Cianni [a,b,c], María de la Mata [a], Francisco J. Delgado [a], Jesús Hernández-Saz [d], Miriam Herrera [a], Sergio I. Molina [a], Michele Giocondo [b,**], Alberto Sanz de León [a,*]

[a] Departamento de Ciencia de los Materiales, I. M. y Q. I, IMEYMAT, Facultad de Ciencias, Universidad de Cádiz, Campus Río San Pedro, s/n, 11510 Puerto Real, Cádiz, Spain
[b] Institute of Nanotechnology, Nanotec Consiglio Nazionale delle Ricerche, Sede di Cosenza, Ponte P. Bucci, Cubo 33C, Rende, 87036, Italy
[c] University of Calabria Physics Department, 87036, Arcavacata di Rende (CS), Italy
[d] Departamento de Ingeniería y Ciencia de los Materiales y del Transporte, Universidad de Sevilla, Avda. Camino de los Descubrimientos s/n, 41092, Sevilla, Spain

A R T I C L E   I N F O

A B S T R A C T

A series of nanocomposites containing gold nanoparticles (AuNPs) are prepared by stereolithography (SL) by simply adding a precursor ($KAuCl_4$) to a photoresist. A thermal treatment is performed after manufacturing the nanocomposites, triggering the reduction of $KAuCl_4$ into AuNPs in solid state. In this approach, the photopolymerization of the resin and the formation of the AuNPs occur independently, allowing the optimization of these two processes separately. Advanced electron microscopy analyses reveal the distribution, size and morphology of the AuNPs synthesized within the resin, showing the influence of the gold precursor concentration and different thermal treatments. The localized surface plasmon resonance (LSPR) of the AuNPs modifies the optical properties of the 3D-printed nanocomposites, yielding transparent yet colored materials even for concentrations as low as 0.1 wt% $KAuCl_4$. This behavior can be modelled by the Mie theory, correlating the macroscopic properties of the nanocomposites with the individual AuNPs embedded in the resin. The possibility of tuning the LSPR of the AuNPs together with the ability of manufacturing 3D-structures with sub-millimeter precision by SL, paves the way for the design of advanced platforms for plasmonics, such as sensors for surface enhanced Raman spectroscopy (SERS).

1. Introduction

Advances in the field of nanotechnology in the last years have evidenced the necessity of finding new strategies to develop new materials that fulfill the high demanding requirements of the market sector as well as their potential scalability at an industrial level. In this context, additive manufacturing (AM) technologies allow the fabrication of 3D objects from a computer-aided design digital file by the layer-by-layer deposition of material without any mold. AM permits the redesign of complex-structured objects with unique functional and mechanical properties, hardly achievable by classical manufacturing techniques [1–3].

Within the different AM technologies, the vat photopolymerization techniques provide higher resolution with competitive printing speeds, rendering high-value products with defined requirements, a key feature in the nanotechnology sector. One of the most widespread technologies is stereolithography (SL), which uses a liquid photoresist (typically epoxy- or acrylate-based). A UV or visible light laser photopolymerizes selectively the uncured resin with a sub-millimeter spot size, reaching printing resolutions down to few microns [4]. The depth of the photopolymerization (also known as the layer height or resolution in the Z axis) can be tuned by varying the laser power, the exposure time, the amount of photoinitiator or using UV absorbers and additives [5,6]. The main limitation of these technologies, however, is the reduced amount of materials suitable for these technologies and the high cost of the system, which may be a concern for some industrial applications [7].

The use of fibers, nanoplates or particles allows obtaining new composite materials suitable for SL with tailored functional and structural properties. The incorporation of these additives must be done carefully to avoid undesired effects as absorption and scattering of the

---

* Corresponding author.
** Corresponding author.
  E-mail addresses: michele.giocondo@cnr.it (M. Giocondo), alberto.sanzdeleon@uca.es (A. Sanz de León).

laser light, known to decrease the resolution, leading to a poor manufacturing of the material with unfinished parts [8,9]. Optimizing the use of these additives makes it possible to obtain materials with improved mechanical and functional properties. For instance, the use of lignin [10], SiO_2 nanoparticles and nanowires [11,12] or graphene oxide [13] has allowed to obtain materials with higher Young's modulus and tensile strength. The manufacturing of Al_2O_3 [14] or $BaTiO_3$ [15] nanocomposites with tailored dielectric properties, or composite materials with ultra-low thermal conductivity [16] have also been reported. This leads the way for improvements in optoelectronics, biotechnology, medicine, or nanotechnology, widening further the possible application fields, permitting high resolution repeatable nanofabrication of 3D complex objects [17,18].

The development of nanocomposites containing metallic nanoparticles for SL has gained attention in the last years. Different authors have proven that copper and silver nanoparticles (AgNPs) can be synthesized *in situ* during the SL process, induced by generation of transient radical species from the photoinitiator present in the SL resin precursor [19–22]. This opens a path to the development of new materials with tunable functional properties. For instance, silver nanocomposites prepared by SL with bactericidal properties [23] or for dielectric applications [24] have been reported.

The use of gold nanoparticles (AuNPs) to obtain SL-printable nanocomposites has been investigated to a lesser extent. Like AgNPs, AuNPs exhibit unique optical properties due to their localized surface plasmon resonance (LSPR), modifying the optical and dielectrical properties of the polymer [25,26]. AuNPs are typically manufactured in solution from different gold precursors via redox reaction in an aqueous medium. This has allowed different researchers to obtain unique geometries with narrow size distributions [27].

Some authors have added these AuNPs onto resins manufactured by SL for catalysis, energy or biomedical applications [28–30] and different works report on the incorporation of AuNPs in the design of polymer nanocomposites by AM to exploit their LSPR for surface enhanced Raman spectroscopy (SERS) applications [31,32]. However, in all these cases, the AuNPs were previously synthesized, *ex situ*. Hinman et al. [33] have alternatively created 3D printed gold nanocomposites for optical detection. In this case, the AuNPs were deposited on the surface after 3D printing by electron-beam evaporation.

These approaches do not allow the *in situ* formation of AuNPs within the 3D-printed material. As an alternative, AuNPs can be formed by applying a simple thermal treatment [34] to inorganic salt precursors embedded within a polymer matrix such as PMMA [35], PVA [36] or PS [37]. When the temperature is increased above a certain threshold, polyhedral AuNPs are obtained, conferring the material with singular optical properties. Among other advantages, the AuNPs synthesis in solid state avoids the use of chemical reagents and eliminates the separation and purification processes, particularly challenging for small-sized AuNPs.

In this work, we study the *in situ* synthesis of AuNPs within an acrylic polymer matrix suitable for SL by applying different thermal treatments after the manufacturing of the object. This approach allows to separate the additive manufacturing of the object from the formation of the AuNPs in two differentiated steps, allowing to tune and control these two processes independently, unlike for AgNPs nanocomposites [21]. The obtained nanocomposites exhibit optical activity caused by the LSPR of the AuNPs, as we demonstrate by UV–Vis spectroscopy, in agreement with the Mie theory. The development of these nanocomposites allows obtaining transparent substrates with plasmonic properties and complex geometries that can be adapted to any surface, which makes them promising candidates for the detection of biomarkers, pollutants or other biomolecules by SERS.

2. Materials and methods

Materials. Potassium tetrachloroaurate (III), ($KAuCl_4$), used as gold

precursor, was purchased from Acros Organics (Belgium). Acrylic resin Form Clear v2 (FLGPCL02, proprietary mixture of photoinitiator and of acrylic monomers and oligomers), used as photoresist, was purchased from Formlabs (USA). Isopropanol was purchased from Scharlab (Spain).

Manufacturing of nanocomposites by stereolithography (SL). A preliminary solubility test was done to determine the maximum amount of $KAuCl_4$ that allows the photopolymerization of the FLGPCL02 acrylic resin by SL, before 3D printing the gold nanocomposites. For this purpose, $KAuCl_4$ concentrations ranging from 0.1 to 2 wt% were tested at different sonication times (15–120 min) in a USC500T Ultrasonic Cleaner.

Then, approximately 50 mL of resin precursors containing 0.1–1 wt% $KAuCl_4$ were prepared for SL by directly dissolving the $KAuCl_4$ into the acrylic resin by sonication for 30 min in order to obtain a homogeneous yellow solution. The precursors were poured onto the SL tank and different objects (25 x 25 × 0.2 mm³ monolayers and 25 x 25 × 2 mm³ parallelepipeds) were manufactured using a SL printer (Form 1+, Formlabs, USA) equipped with a 405 nm laser with an output power of 120 mW and a spot size of 140 μm. A plastic spatula was used to remove the objects from the build platform after they were completely printed. The objects were then washed in isopropanol for at least 15 min to remove possible unreacted monomers from the resin and UV-postcured for 60 min at room temperature inside a UV-chamber (FormCure, Formlabs, USA) equipped with a light source of 405 nm and power of 1.25 mW/cm².

***In situ* synthesis of the gold nanoparticles (AuNPs).** The AuNPs were synthesized by a subsequent treatment in solid state after the objects were 3D-printed and the resin was fully cured. Two different approaches were studied. On the one hand, a thermal post-curing at temperatures up to 170 °C inside an oven was investigated. Alternatively, the samples underwent a post-processing combining temperature with UV radiation inside the FormCure chamber at temperatures up to 80 °C. For comparative purposes, both treatments were carried out for 60 min. The color change of the composites indicated the successful formation of the AuNPs. A summary of the whole fabrication process can be found in Fig. 1.

Characterization. The different nanocomposites manufactured were characterized via scanning electron microscopy (SEM) and transmission electron microscopy (TEM). SEM measurements were performed using a FEI Nova NanoSEM 450 microscope equipped with a field-emission gun for high-resolution analyses. TEM specimens were obtained by focused ion beam (FIB) milling and lift-out in a Thermo Fisher Scientific Scios2 Dual Beam SEM/FIB system [38]. Low keV milling was used to ensure the structural integrity of the nanocomposite. High angle annular dark field (HAADF) analyses were performed at a FEI Titan Cube transmission electron microscope provided with a X-FEG Schottky electron gun and equipped with a Cs-probe corrector and a Gatan Dual EELS spectrometer, operated at 200 kV under STEM mode conditions using 0.25 eV/ch for EELS Spectrum Imaging. A Thermo Scientific TALOS F200S (Thermo Fisher Scientific, Waltham, MA, USA) microscope working at 200 kV has been used to obtain the EDX spectra and the images for the electron tomography analyses. Twenty-nine HAADF-STEM images were acquired over an angular range of 140° with a tilting step of 5°. The tilt series were accurately aligned using the Inspect 3D software of Thermo Fisher Scientific Company with the cross-correlation method. The 3D reconstruction was carried out using the simultaneous iterative reconstruction technique and was visualized with the software AVIZO for FEI systems (Materials Science) 9.9.1. Differential scanning calorimetry (DSC) experiments were performed in a Q20 (T&A Instruments, USA). Temperature sweeps were performed from room temperature to 200 °C at a rate of 10 °C/min under nitrogen flow. A subsequent cooling and heating sweep at 10 °C/min was performed to confirm all the resin was cured in the first sweep. Thermogravimetric analysis (TGA) was carried out in a Q50 (T&A Instruments, USA). A temperature sweep was performed from room temperature to
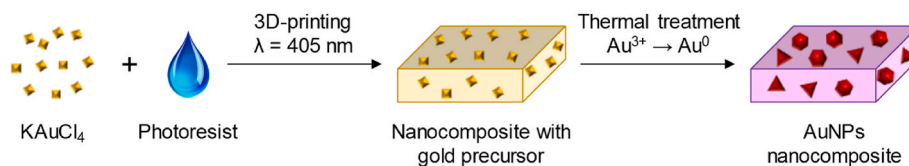
Fig. 1. Scheme of the additive manufacturing of the Au nanocomposites.

600 °C at a rate of 10 °C/min under nitrogen flow. The optical properties of the nanocomposites were studied by UV–Vis spectroscopy. For this purpose, the absorbance of the nanocomposites was monitored in the range of 300–800 nm using a Varian Cary 50 Conc UV–Vis spectrophotometer. At least three different samples were analyzed in all cases.

3. Results and discussion

Preliminary tests were done to identify the range of $KAuCl_4$ concentrations soluble in the photoresist. For this purpose, different amounts of $KAuCl_4$ (from 0.1 to 2 wt%) were dissolved in the resin precursor by sonicating at different times. It was observed that for concentrations below 1 wt%, 15 min of sonication were enough to dissolve properly the inorganic salt in the resin, obtaining a homogeneous yellow solution. 1 wt% $KAuCl_4$ precursor required longer sonication times (at least 30 min) and 2 wt% $KAuCl_4$ was not completely dissolved even for longer sonication times, indicating that the solubility limit of $KAuCl_4$ in the resin is between 1 and 2 wt%.

Hence, the 0.1–1 wt% $KAuCl_4$ resins were initially selected for SL. However, objects could not be properly printed for mixtures with more than 0.5 wt% $KAuCl_4$, probably because of partial laser absorption due to the presence of $KAuCl_4$. In fact, when concentration was set to 0.5 wt%, only monolayers were successfully printed. This concentration allows the polymerization of the first layer but probably absorbs enough laser light to hinder the polymerization of a subsequent layer during the SL process. Therefore, 0.5 wt% $KAuCl_4$ was set as the upper concentration threshold that allows printing these nanocomposites. 20×20 mm^2 monolayers (200 μm height) containing 0.1, 0.3 and 0.5 wt% $KAuCl_4$ were printed. The monolayers were UV post-cured at room temperature for 60 min to ensure that the resin is fully polymerized [13]. After this process, the monolayers remained transparent, indicating that this post-processing does not reduce the $KAuCl_4$ into AuNPs. Previous studies indicate that Au^{3+} embedded in a polymer matrix can be reduced into AuNPs in solid state when the temperature is increased [34,35] so a thermal treatment without any UV source at different temperatures was tested. The temperature was increased from room temperature up to 180 °C in intervals of 10 °C and each temperature was fixed for 60 min. For temperatures below 170 °C, no change in color was observed, indicating that there is no significant AuNPs formation, if any. However, after 60 min at 170 °C, the monolayer underwent a color change and presented a homogeneous, intense pink color (Fig. 2a)). Increasing the

temperature to 180 °C did not lead to any further change in color. SEM analysis of the monolayers evidenced the presence of AuNPs at the composites surface (Fig. 2b–c)). A good distribution of AuNPs with different polygonal morphologies is observed after the thermal treatment, in agreement with previous studies [36,37,39]. An alternative post-processing by combining UV light and temperature was also assessed. The monolayers containing 0.1 wt% $KAuCl_4$ also experienced a color change after heating at 80 °C in presence of UV light for 60 min (Fig. 3a)). In contrast with the treatment in absence of UV light, the surface of the nanocomposites exposed to UV (Fig. 3b–c)) showed an uneven AuNPs distribution, agglomerated into larger structures that reach sizes above 1 μm, likely responsible for the subtler color change. In this case, the monolayers exhibit a more blueish color, in agreement with the presence of larger AuNPs (or their agglomerates) [26]. Thus, even though UV radiation triggers the reduction of $KAuCl_4$, the resulting composites do not show homogeneous distribution of AuNPs. Hence, for the following experiments, all the Au nanocomposites will be treated at 170 °C for 60 min in absence of UV light.

Fig. 4 shows the influence of the $KAuCl_4$ concentration in the size and shape of the AuNPs contained in the SL printed monolayers. All the images have the same magnification for direct comparison. Interestingly, when the $KAuCl_4$ concentration is increased from 0.1 to 0.5 wt%, the number of AuNPs decreases, while they become bigger. This suggests that higher amounts of gold precursor do not lead to the formation of more individual AuNPs. Instead, it is likely that the former AuNPs created act as nucleation seeds for the further reduction of Au^{3+} cations entrapped in the polymeric matrix into Au^0 increasing the size of the nanoparticles following an autocatalytic growth mechanism [40,41].

A quantitative analysis of the AuNPs for this concentrations range is presented in Fig. 4d). As already discussed, the higher the salt precursor content, the larger the AuNPs. The mean values measured are 91 ± 37 nm, 175 ± 60 nm and 198 ± 52 nm for 0.1, 0.3 and 0.5 wt% $KAuCl_4$ nanocomposites, respectively. In all cases, there are some outliers with sizes significantly above and below the average values. The bigger AuNPs may be originated from the coalescence of individual nanoparticles that have merged into bigger ones. Also, smaller AuNPs with sizes below 50 nm can be identified, close to the attainable spatial resolution during SEM measurements. In general, it can be concluded that the polydispersity of the AuNPs is smaller for the nanocomposites prepared with 0.1 wt% $KAuCl_4$, as it can be extracted from the different error bars of the box plots.
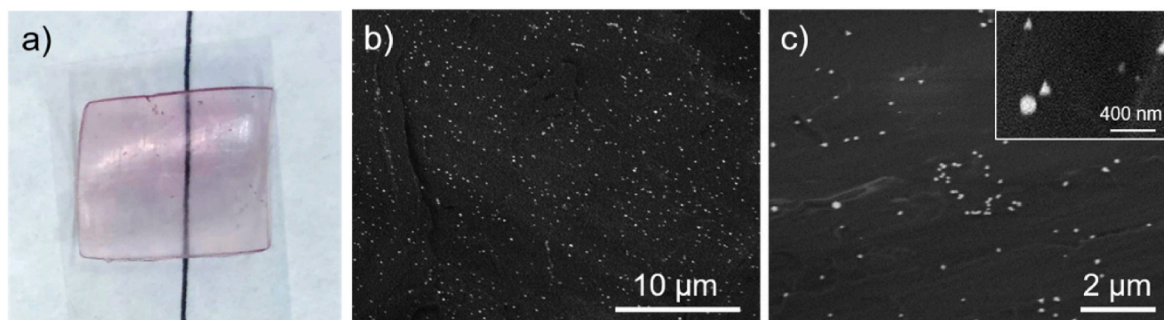

Fig. 2. a) Digital picture and b), c) SEM micrographs of a 0.1 wt% $KAuCl_4$ nanocomposite monolayer (200 μm thickness) printed by SL and treated at 170 °C for 60 min. Inset in c) shows some AuNPs with different nanocrystal shapes.
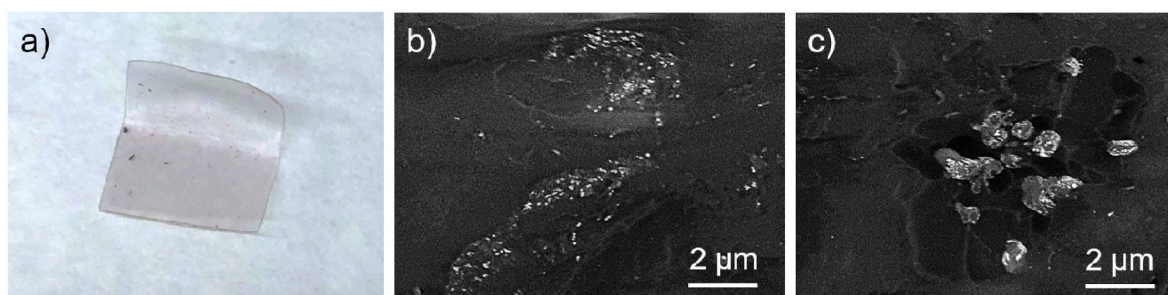
Fig. 3. a) Digital picture and b), c) SEM micrographs of a 0.1 wt% KAuCl$_4$ nanocomposite monolayer (200 μm thickness) printed by SL and treated at 80 °C for 60 min in presence of UV light.
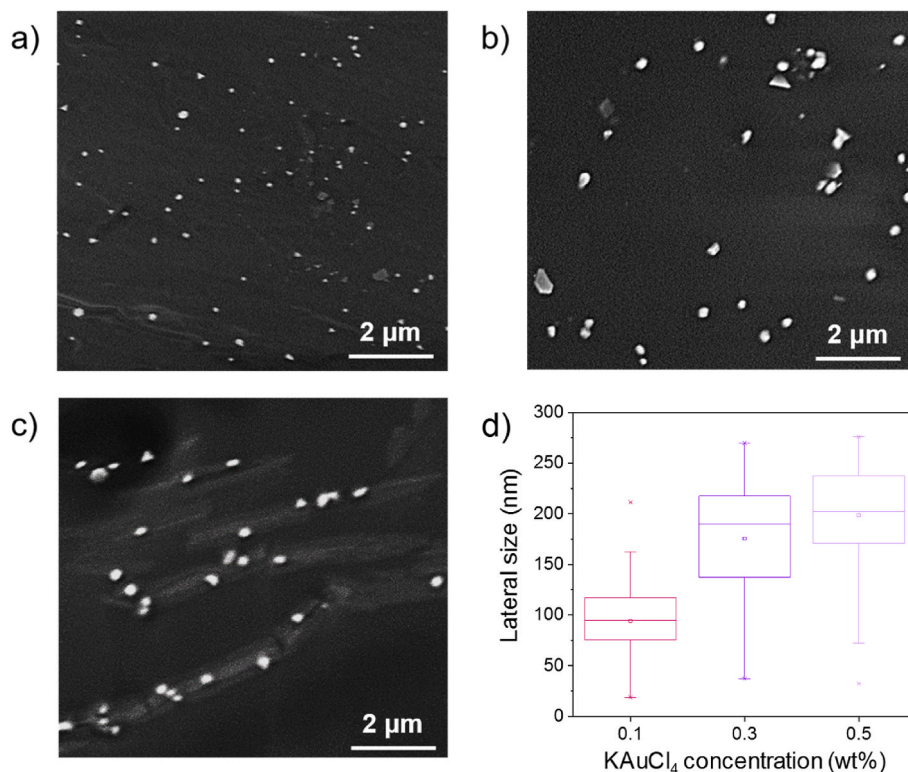

Fig. 4. SEM micrographs of a) 0.1 wt% KAuCl$_4$, b) 0.3 wt% KAuCl$_4$ and c) 0.5 wt% KAuCl$_4$ nanocomposite monolayers printed by SL after post-processing at 170 °C for 60 min; d) box plots depicting the influence of the KAuCl$_4$ concentration in the AuNPs lateral size.

The thermal stability of the nanocomposites was studied by DSC and TGA. The DSC thermograms in Fig. 5a) show a glass transition temperature (T$_g$) around 60 °C for all the cases studied. In particular, a T$_g$ of 57.3, 62.8, 63.0 and 64.2 °C was observed for the pristine resin and the 0.1, 0.3, 0.5 wt% KAuCl$_4$ nanocomposites, respectively. This seems to indicate a contribution from the AuNPs to increase the T$_g$ of the material. The degree of cure of the resin was obtained from the transitions observed at 150–180 °C, in agreement with our previous studies [8,21]. However, it is not observed a clear exothermic peak (attributed to the residual curing enthalpy) in none of these thermograms, so it is assumed that practically a full degree of cure has been achieved in all cases. Instead, it is observed a series of T$_g$ around 170 °C, more or less pronounced. These transitions include a slightly endothermic peak, which can be ascribed to the aging of polymer resin [42]. As this behavior is also observed in the pristine resin, it does not seem to be related with the formation of the AuNPs. These findings are supported by the TGA results presented in Fig. 5b), where a small increase of the thermal stability of all the nanocomposites is observed when compared to the pristine resin, even though these differences are not particularly significant. It was not

observed any transition attributable to the thermal decomposition of KAuCl$_4$ into AuNPs, likely because the amount of gold precursor is very low for all the nanocomposites prepared. These results evidence that the AuNPs do not affect the thermal stability of the material due to their low amount and good dispersion in the resin matrix.

To gain more information about the optical properties of 3D printed Au nanocomposites, a parallelepiped (20 x 20 × 10 mm^3, 50 layers) was printed with a layer height of 200 μm and a concentration of 0.1 wt% KAuCl$_4$. In these conditions, the object looked completely transparent and colorless after being printed (Fig. 6a)). The sample did not vary its color or transparency after 60 min of UV light at room temperature, supporting that this UV treatment is not enough to form AuNPs. Only after a subsequent thermal treatment for 60 min at 170 °C the parallelepiped showed an intense, dark pink color when light is reflected (Fig. 6b)). This color slightly changes towards violet with transmitted light (Fig. 6c)), evidencing the characteristic optical properties of the AuNPs caused by their LSPR. Sample is colored yet transparent, since the AuNPs formed possess sizes below 400 nm, i.e. below the visible wavelength range. As Fig. 6d) illustrates, the text behind the 10 mm
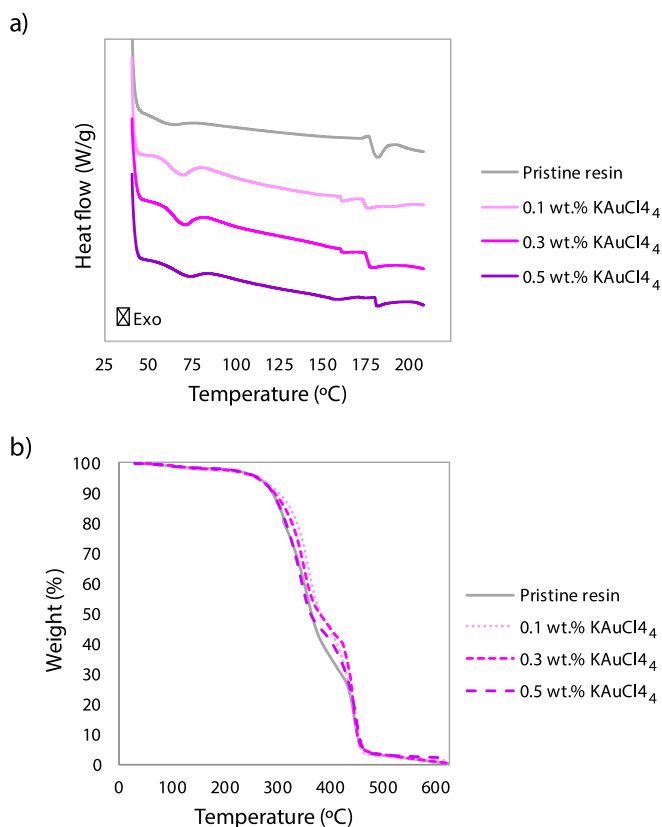
a)

b)

Fig. 5. a) DSC and b) TGA thermograms of the pristine resin, 0.1 wt% KAuCl$_4$, 0.3 wt% KAuCl$_4$ and 0.5 wt% KAuCl$_4$ nanocomposite monolayers printed by SL after post-processing at 170 °C for 60 min.

thickness object can be easily read. The color change occurred in a similar way to the previously printed monolayers.

Fig. 7a) depicts two different regions of the 3D-printed parallelepiped studied by SEM and TEM. In order to analyze the bulk material (i. e., avoiding the surfaces) by TEM, an electron-transparent lamella was obtained by FIB from the nanocomposite. The materials were studied under HAADF conditions rendering images with chemical contrast attending to the atomic number of the constituents, thus reproducing the AuNPs brighter than the polymeric matrix. The parallelepiped surface examined by SEM (Fig. 7b)) did not present significant differences compared to the printed monolayers (Fig. 4a)). Fig. 7c shows a HAADF image of the 0.1 wt% KAuCl$_4$ nanocomposite, where several NPs can be observed, homogeneously distributed within the polymer matrix STEM-EDX analyses (Fig. 7d) reveal the presence of C, O (both attributed to the polymer matrix), Au (due to the presence of AuNPs), as well as Cu from the TEM grid. Neither Cl nor K (at 2.6 or 3.3 keV, respectively) were detected, demonstrating the absence of the gold precursor. EELS chemical mapping presented in Fig. 7e) confirms the Au composition of the NPs. These AuNPs present a distribution with sizes of 26 ± 8 nm, below those previously observed at the nanocomposite surface.

HAADF higher magnification images presented in Fig. 8a–c) evidence that the nanoparticles are faceted. In order to obtain 3D information on the morphology of these AuNPs, electron tomography was carried out in the AuNP of Fig. 8c), and an image of the 3D reconstruction is included in Fig. 8d) (see also Supporting **Video**). This analysis showed that the AuNP is isotropic and polyhedral, presenting multiple facets, in agreement with previous studies where the growth of different isotropic AuNPs are formed from small gold precursors or nanoclusters [43,44]. Complementary EDX mapping analysis of this AuNP is also presented in Fig. 8e).

The differences found between the surface and the interior of the gold nanocomposite may be due to several reasons. First, it is worth noting that SEM has poorer spatial resolution than (S)TEM, therefore small AuNPs on the surface of the material would not be detected by SEM. On the other hand, AuNPs as large as those found by SEM at the nanocomposite surface were not definitely observed inside the bulk material. It is likely that there are surface effects caused by differences in the diffusion of the gold precursor in solid state that lead to the formation of larger AuNPs, even with different morphology, on the surface of the composites than inside of the resin. Previous works report a similar behavior in AgNPs nanocomposites prepared by classical photopolymerization [45], SL [21] and digital light processing (DLP) [24, 46]. Even though these mechanisms are not fully understood, the authors state that the different sizes and morphology can be ascribed to the
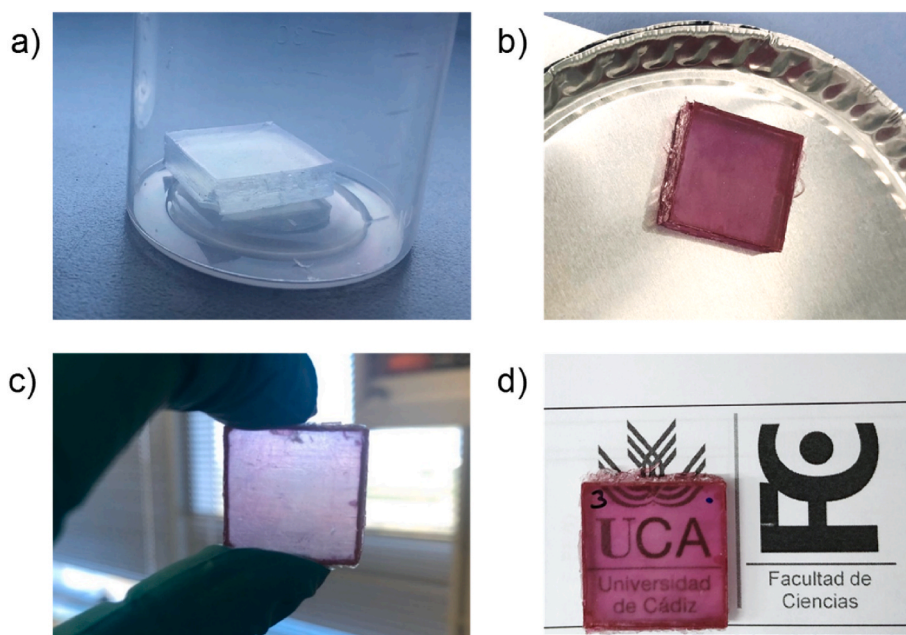

Fig. 6. Digital images of a 0.1 wt% KAuCl$_4$ nanocomposite parallelepiped (20 x 20 × 10 mm^3) a) right after printing (no thermal treatment); after thermal treatment at 170 °C for 60 min b) under reflected white light; c) under transmitted white light and d) on top of a text to illustrate its degree of transparency.
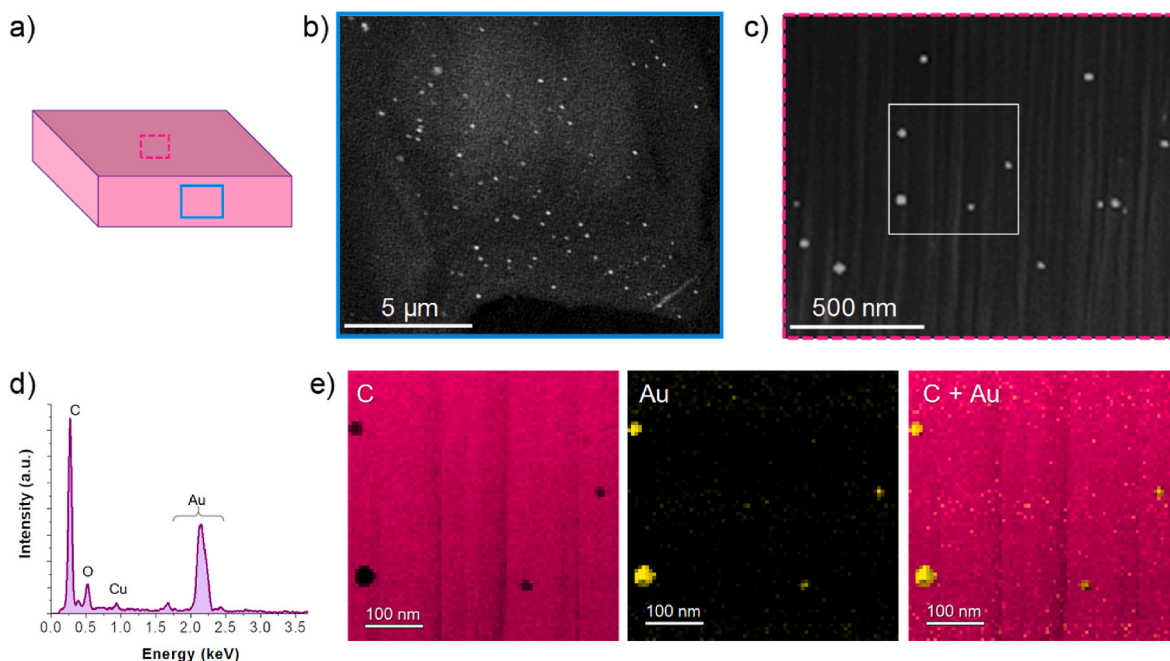
Fig. 7. a) Cartoon depicting the region where b) SEM (blue rectangle) and c) HAADF (dashed pink rectangle) images were taken from a 0.1 wt% $KAuCl_4$ nanocomposite parallelepiped (20 x 20 × 10 mm³) treated at 170 °C for 60 min; d) EDX average spectrum and e) EELS maps taken from c). C and Au are displayed in magenta and yellow, respectively. (For interpretation of the references to color in this figure legend, the reader is referred to the Web version of this article.)
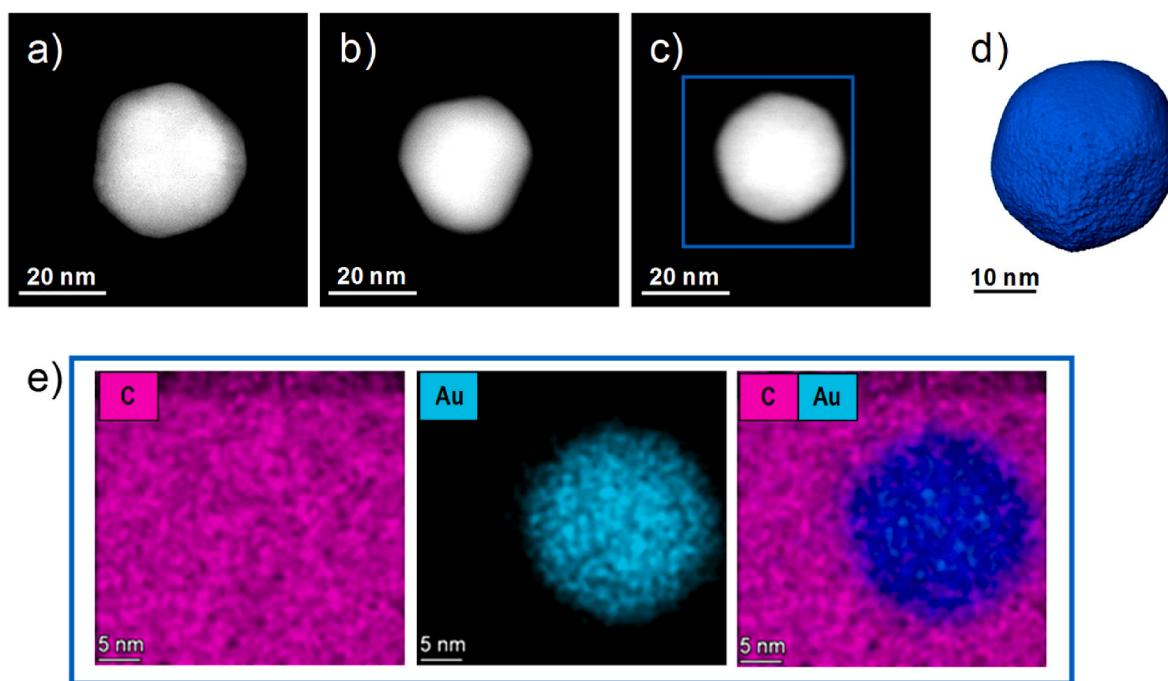

Fig. 8. a-c) HAADF high-magnification images of individual AuNPs of a 0.1 wt% $KAuCl_4$ nanocomposite parallelepiped (20 x 20 × 10 mm³) treated at 170 °C for 60 min; d) 3D-reconstruction and e) EDX mapping of the AuNP displayed in c).

diffusion of the precursors or NPs during the nanocomposite manufacturing or post-processing, differences of light penetration in the sample or oxidation events happening selectively at the material surface when it is subjected to high temperatures.

Finally, the macroscopic optical properties of these nanocomposites were studied by UV–Vis spectrometry. Fig. 9a) shows the spectra of 0.1 wt% $KAuCl_4$ nanocomposite parallelepipeds under different conditions. Before any post-processing with temperature, the nanocomposites are fully transparent, presenting transmittance values around 70% for wavelengths above 430 nm. Even though there is some light scattering, these values evidence that the samples possess a high degree of transparency in practically the entire visible range. Below 430 nm, the amount of light absorbed (or scattered) increases dramatically because of the polymer resin, which constitutes the 99.9 wt% of the nanocomposite. These values are similar to those obtained for the pristine resin, indicating that the gold precursor does not interfere with the
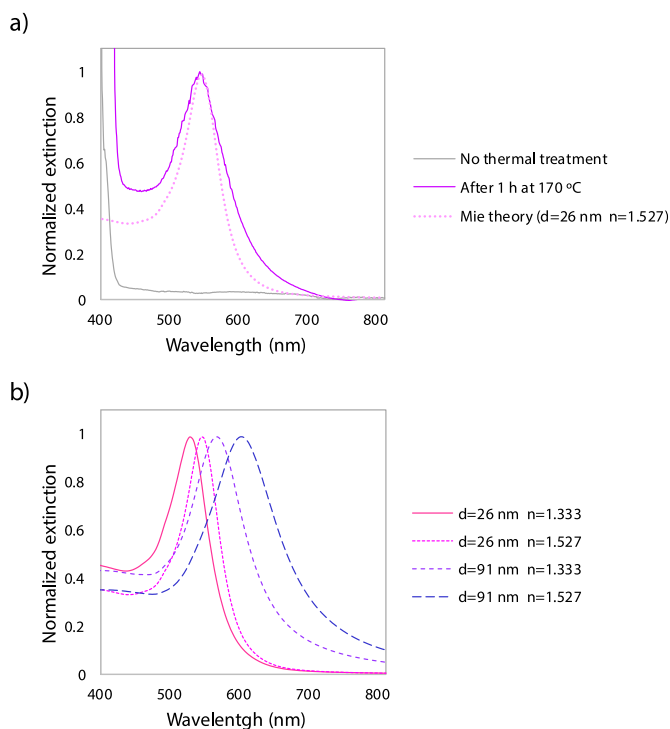
a)

b)

Fig. 9. a) UV–Vis spectra of a 0.1 wt% KAuCl$_4$ nanocomposite parallelepiped (20 x 20 × 10 mm^3) without any thermal treatment (grey curve) and after 60 min at 170 °C (pink curve). The curve predicted by the Mie theory for spherical, 26 nm sized nanoparticles in a medium with a refractive index $n = 1.527$ is also presented as a pink, dashed curve; b) extinction curves predicted by the Mie theory for spherical AuNPs with diameters d of 26 and 91 nm, homogeneously dispersed in a medium with refractive index n of 1.333 (water) and 1.527 (polymer resin). (For interpretation of the references to color in this figure legend, the reader is referred to the Web version of this article.)

transparency of the material in the visible range. After the thermal treatment at 170 °C for 60 min, the 0.1 wt% KAuCl$_4$ nanocomposites show a peak with a maximum value at 548 ± 6 nm. This curve is characteristic of AuNPs with sizes below 100 nm, which possess optical activity due to their LSPR in the range of the visible light [47]. This behavior can be modelled by the Mie theory. Briefly, it states that the color (i.e. the maximum of the absorbance in the visible light spectrum) depends on the size of the AuNPs and the refractive index of the medium where they are dispersed [48,49]. In general, AuNPs are homogeneously dispersed in water ($n = 1.333$) but in our case, they are embedded in a polymeric resin with higher refractive index ($n = 1.527$) [50], which is also expected to modify their optical behavior. Considering this, and simplifying the AuNPs morphology as spherical, the best fit for the Mie theory occurs when the AuNPs possess average diameters around 30 nm. In Fig. 9a) a dashed curve is presented with the prediction by the Mie theory for 26 nm AuNPs, in agreement with the results obtained by TEM, and $n = 1.527$. The experimental curve has a broader distribution, likely due to the unavoidable size dispersion of the experimental AuNPs, which contributes to widen the observed UV–Vis peak, but the local maximum and the shape are well-reproduced. Fig. 9b) presents different curves predicted by the Mie theory for different refractive indices and using the AuNPs average size values observed by SEM (91 nm). A decrease in the refractive index of the medium shifts the LSPR of the AuNPs to lower wavelengths. An increase in the average AuNPs size red-shifts the LSPR peak, while it also becomes broader, having a mismatch with the experimental results. This confirms that the optical behavior of these nanocomposites is governed by the AuNPs embedded within the polymer matrix, as observed by TEM, while the formation of larger AuNPs occurs locally at the material surface. It also proves that

the number of larger AuNPs is significantly lower and they practically do not contribute to the macroscopic optical properties, in agreement with the experimental UV–Vis spectrum. Hence, these high-resolution microscopy analyses are critical for a proper understanding of the functional behavior of these nanocomposites and the correlation of the macroscopic properties with the microstructure of the material.

4. Conclusions

In this work we have developed a series of nanocomposites containing AuNPs of different sizes and morphologies, which gives them unique plasmonic properties. We have proven that the 3D-printing of the nanocomposites by SL can be separated from the synthesis of the AuNPs in two different, well-differentiated steps. First, the photoresist is cured by SL using a UV laser. A post-processing step inside a UV chamber ensures the full photopolymerization of the resin. The gold precursor, KAuCl$_4$, does not interfere with any of these processes. Then, a thermal treatment is carried out. In this process, AuNPs are formed after 60 min when the temperature is set to 170 °C. This is a promising alternative to classical synthesis of AuNPs via redox reaction in solution, simplifying the process and avoiding the use of solvents, surfactants, chemicals or further purification and separation steps. Electron microscopy analyses of the 0.1 wt% KAuCl$_4$ nanocomposites showed that the AuNPs have polyhedral morphologies and are bigger at the nanocomposites surface (91 ± 37 nm) than within the material (26 ± 8 nm). The overall macroscopic optical properties of the nanocomposites are governed by the LSPR of the smaller AuNPs, in good agreement with the Mie theory. Therefore, this study evidences the need to carefully characterize these nanocomposites, where nanoparticles are formed *in situ* within the polymer matrix.

These nanocomposites have potential applications as versatile tools for SERS detection, especially for non-destructive assays on non-planar substrates, such as elements of cultural heritage. We anticipate that these nanocomposites will pave the way for the design of advanced platforms for plasmonics, where tailor-made objects with precise geometries and sub-millimeter resolution are required.

Author contributions

Conceptualization: WDC, ASdL; Formal analysis: WDC; Validation: MG, ASdL; Investigation: WDC, MdlM, FJD, JHS, MH; Writing – original draft: WDC; Writing – review and editing: MdlM, MH, SIM, MG, ASdL; Supervision: SIM, MG, ASdL; Funding acquisition: MdlM, SIM, MG, ASdL.

Declaration of competing interest

The authors declare that they have no known competing financial interests or personal relationships that could have appeared to influence the work reported in this paper.

Data availability

Data will be made available on request.

UCA.

Appendix A. Supplementary data

Supplementary data to this article can be found online at https://doi.org/10.1016/j.polymertesting.2022.107869.

References

[1] O. Ivanova, C. Williams, T. Campbell, Additive manufacturing (AM) and nanotechnology: promises and challenges, Rapid Prototyp. J. 19 (2013) 353–364, https://doi.org/10.1108/RPJ-12-2011-0127.

[2] S.A.M. Tofail, E.P. Koumoulos, A. Bandyopadhyay, S. Bose, L. O'Donoghue, C. Charitidis, Additive manufacturing: scientific and technological challenges, market uptake and opportunities, Mater. Today 21 (2018) 22–37, https://doi.org/10.1016/j.mattod.2017.07.001.

[3] L.J. Tan, W. Zhu, K. Zhou, Recent progress on polymer materials for additive manufacturing, Adv. Funct. Mater. 30 (2020), 2003062, https://doi.org/10.1002/adfm.202003062.

[4] V. Hahn, P. Kiefer, T. Frenzel, J. Qu, E. Blasco, C. Barner-Kowollik, M. Wegener, Rapid assembly of small materials building blocks (voxels) into large functional 3D metamaterials, Adv. Funct. Mater. 30 (2020), 1907795, https://doi.org/10.1002/adfm.201907795.

[5] Z. Weng, Y. Zhou, W. Lin, T. Senthil, L. Wu, Structure-property relationship of nano enhanced stereolithography resin for desktop SLA 3D printer, Composer Part A Appl. Sci. Manuf. 88 (2016) 234–242, https://doi.org/10.1016/j.compositesa.2016.05.035.

[6] Y. Yang, L. Li, J. Zhao, Mechanical property modeling of photosensitive liquid resin in stereolithography additive manufacturing: bridging degree of cure with tensile strength and hardness, Mater. Des. 162 (2019) 418–428, https://doi.org/10.1016/j.matdes.2018.12.009.

[7] X. Wang, M. Jiang, Z. Zhou, J. Gou, D. Hui, 3D printing of polymer matrix composites: a review and prospective, Compos. B Eng. 110 (2017) 442–458, https://doi.org/10.1016/j.compositesb.2016.11.034.

[8] A.S. De León, S.I. Molina, Influence of the degree of cure in the bulk properties of graphite nanoplatelets nanocomposites printed via stereolithography, Polymers 12 (2020) 1103, https://doi.org/10.3390/polym12051103.

[9] Q. Ma, Y. Zhang, V. Launay, S. Liu, J. Lalevée, How to overcome the light penetration issue in photopolymerization? An example for the preparation of high content iron-containing opaque composites and application in 3D printing, Eur. Polym. J. 165 (2022), 111011, https://doi.org/10.1016/j.eurpolymj.2022.111011.

[10] S. Zhang, M. Li, N. Hao, A.J. Ragauskas, Stereolithography 3D printing of lignin-reinforced composites with enhanced mechanical properties, ACS Omega 4 (2019) 20197–20204, https://doi.org/10.1021/acsomega.9b02455.

[11] M. Invernizzi, R. Suriano, A. Muscatello, S. Turri, M. Levi, Near-visible stereolithography of a low shrinkage cationic/free-radical photopolymer blend and its nanocomposite, J. Appl. Polym. Sci. 137 (2020), 48333, https://doi.org/10.1002/app.48333.

[12] T. Ritacco, W. Di Cianni, D. Perziano, P. Magarò, A. Convertino, C. Maletta, A. De Luca, A. Sanz de León, M. Giocondo, High-resolution 3D fabrication of glass fiber-reinforced polymer nanocomposite (FRPN) objects by two-photon direct laser writing, ACS Appl. Mater. Interfaces 14 (2022) 17754–17762, https://doi.org/10.1021/acsami.1c21708.

[13] A.S. de León, M. de la Mata, F.J. Delgado, S.I. Molina, Printable graphene oxide nanocomposites as versatile platforms for immobilization of functional biomolecules, Macromol. Mater. Eng. 307 (2022), 2100784, https://doi.org/10.1002/mame.202100784.

[14] M. Kurimoto, Y. Yamashita, H. Ozaki, T. Kato, T. Funabashi, Y. Suzuoki, 3D printing of conical insulating spacer using alumina/UV-cured-resin composite, IEEE Conf. Electr. Insul. Dielectr. Phenom. (2015) 463–466, https://doi.org/10.1109/CEIDP.2015.7352047, 2015.

[15] W. Wang, J. Sun, B. Guo, X. Chen, K.P. Ananth, J. Bai, Fabrication of piezoelectric nano-ceramics via stereolithography of low viscous and non-aqueous suspensions, J. Eur. Ceram. Soc. 40 (2020) 682–688, https://doi.org/10.1016/j.jeurceramsoc.2019.10.033.

[16] M. He, Y. Zhao, B. Wang, Q. Xi, J. Zhou, Z. Liang, 3D printing fabrication of amorphous thermoelectric materials with ultralow thermal conductivity, Small 11 (2015) 5889–5894, https://doi.org/10.1002/smll.201502153.

[17] Z. Guo, A.A. Poot, D.W. Grijpma, Advanced polymer-based composites and structures for biomedical applications, Eur. Polym. J. 149 (2021), 110388, https://doi.org/10.1016/j.eurpolymj.2021.110388.

[18] A. Al Rashid, W. Ahmed, M.Y. Khalid, M. Koç, Vat photopolymerization of polymers and polymer composites: processes and applications, Addit. Manuf. 47 (2021), 102279, https://doi.org/10.1016/j.addma.2021.102279.

[19] G. Taormina, C. Sciancalepore, F. Bondioli, M. Messori, Special resins for stereolithography: in situ generation of silver nanoparticles, Polymers (2018) 10, https://doi.org/10.3390/polym10020212.

[20] İ. Aktitiz, R. Varol, N. Akkurt, M.F. Saraç, In-situ synthesis of 3D printable mono- and Bi-metallic (Cu/Ag) nanoparticles embedded polymeric structures with enhanced electromechanical properties, Polym. Test. 90 (2020), https://doi.org/10.1016/j.polymertesting.2020.106724.

[21] L.M. Valencia, M. Herrera, M. de la Mata, A.S. de León, F.J. Delgado, S.I. Molina, Synthesis of silver nanocomposites for stereolithography: in situ formation of nanoparticles, Polymers 14 (2022) 1168, https://doi.org/10.3390/polym14061168.

[22] C. Sciancalepore, F. Moroni, M. Messori, F. Bondioli, Acrylate-based silver nanocomposite by simultaneous polymerization–reduction approach via 3D stereolithography, Compos. Commun. 6 (2017) 11–16, https://doi.org/10.1016/j.coco.2017.07.006.

[23] G.A. González Flores, V. Bertana, A. Chiappone, I. Roppolo, L. Scaltrito, S. L. Marasso, M. Cocuzza, G. Massaglia, M. Quaglio, C.F. Pirri, S. Ferrero, Single-step 3D printing of silver-patterned polymeric devices for bacteria proliferation control, Macromol. Mater. Eng. 307 (2022), 2100596, https://doi.org/10.1002/mame.202100596.

[24] E. Fantino, A. Chiappone, F. Calignano, M. Fontana, F. Pirri, I. Roppolo, In situ thermal generation of silver nanoparticles in 3D printed polymeric structures, Materials 9 (2016) 21–23, https://doi.org/10.3390/ma9070589.

[25] K.L. Kelly, E. Coronado, L.L. Zhao, G.C. Schatz, The optical properties of metal nanoparticles: the influence of size, shape, and dielectric environment, J. Phys. Chem. B 107 (2003) 668–677, https://doi.org/10.1021/jp026731y.

[26] M.B. Ross, C.A. Mirkin, G.C. Schatz, Optical properties of one-, two-, and three-dimensional arrays of plasmonic nanostructures, J. Phys. Chem. C 120 (2016) 816–830, https://doi.org/10.1021/acs.jpcc.5b10800.

[27] J.E. Ortiz-Castillo, R.C. Gallo-Villanueva, M.J. Madou, V.H. Perez-Gonzalez, Anisotropic gold nanoparticles: a survey of recent synthetic methodologies, Coord. Chem. Rev. 425 (2020), 213489, https://doi.org/10.1016/j.ccr.2020.213489.

[28] G.N. Abdelrasoul, B. Farkas, I. Romano, A. Diaspro, S. Beke, Nanocomposite scaffold fabrication by incorporating gold nanoparticles into biodegradable polymer matrix: synthesis, characterization, and photothermal effect, Mater. Sci. Eng. C 56 (2015) 305–310, https://doi.org/10.1016/j.msec.2015.06.037.

[29] A. Zsedenyi, B. Farkas, G.N. Abdelrasoul, I. Romano, E. Gyukity-Sebestyen, K. Nagy, M. Harmati, G. Dobra, S. Kormondi, G. Decsi, J.-H. Yoo, S. Shin, X. Lepró, B.D. Moran, C.M. Aracne-Ruddle, T.F. Baumann, O.S. Jones, J. Biener, A simple, highly efficient route to electroless gold plating on complex 3D printed polyacrylate plastics, Chem. Commun. 54 (2018) 10463–10466, https://doi.org/10.1039/C8CC05368E.

[30] S.H. Kim, J.A. Jackson, J.S. Oakdale, J.-B. Forien, J.M. Lenhardt, J.-H. Yoo, S. Shin, X. Lepró, B.D. Moran, C.M. Aracne-Ruddle, T.F. Baumann, O.S. Jones, J. Biener, A simple, highly efficient route to electroless gold plating on complex 3D printed polyacrylate plastics, Chem. Commun. 54 (2018) 10463–10466, https://doi.org/10.1039/C8CC05368E.

[31] J. Langer, D. Jimenez de Aberasturi, J. Aizpurua, R.A. Alvarez-Puebla, B. Auguié, J. J. Baumberg, G.C. Bazan, S.E.J. Bell, A. Boisen, A.G. Brolo, J. Choo, D. Cialla-May, V. Deckert, L. Fabris, K. Faulds, F.J. García de Abajo, R. Goodacre, D. Graham, A. J. Haes, C.L. Haynes, C. Huck, T. Itoh, M. Käll, J. Kneipp, N.A. Kotov, H. Kuang, E. C. Le Ru, H.K. Lee, J.-F. Li, X.Y. Ling, S.A. Maier, T. Mayerhöfer, M. Moskovits, K. Murakoshi, J.-M. Nam, S. Nie, Y. Ozaki, I. Pastoriza-Santos, J. Perez-Juste, J. Popp, A. Pucci, S. Reich, B. Ren, G.C. Schatz, T. Shegai, S. Schlücker, L.-L. Tay, K. G. Thomas, Z.-Q. Tian, R.P. Van Duyne, T. Vo-Dinh, Y. Wang, K.A. Willets, C. Xu, H. Xu, Y. Xu, Y.S. Yamamoto, B. Zhao, L.M. Liz-Marzán, Present and future of surface-enhanced Raman scattering, ACS Nano 14 (2020) 28–117, https://doi.org/10.1021/acsnano.9b04224.

[32] J. Plou, B. Molina-Martínez, C. García-Astrain, J. Langer, I. García, A. Ercilla, G. Perumal, A. Carracedo, L.M. Liz-Marzán, Nanocomposite scaffolds for monitoring of drug diffusion in three-dimensional cell environments by surface-enhanced Raman spectroscopy, Nano Lett. 21 (2021) 8785–8793, https://doi.org/10.1021/acs.nanolett.1c03070.

[33] S.S. Hinman, K.S. McKeating, Q. Cheng, Plasmonic sensing with 3D printed optics, Anal. Chem. 89 (2017) 12626–12630, https://doi.org/10.1021/acs.analchem.7b03967.

[34] K. Otto, I. Oja Acik, M. Krunks, K. Tõnsuaadu, A. Mere, Thermal decomposition study of HAuCl4.3H2O and AgNO3 as precursors for plasmonic metal nanoparticles, J. Therm. Anal. Calorim. 118 (2014) 1065–1072, https://doi.org/10.1007/s10973-014-3814-3.

[35] D. Wostek-Wojciechowska, J.K. Jeszka, C. Amiens, B. Chaudret, P. Lecante, The solid-state synthesis of metal nanoparticles from organometallic precursors, J. Colloid Interface Sci. 287 (2005) 107–113, https://doi.org/10.1016/j.jcis.2005.01.109.

[36] S. Porel, S. Singh, T.P. Radhakrishnan, Polygonal gold nanoplates in a polymer matrix, Chem. Commun. (2005) 2387–2389, https://doi.org/10.1039/B500536A.

[37] A.S. de León, M. de la Mata, S.I. Molina, Hybrid hierarchically structured materials combining breath figures and thermal decomposition of KAuCl4, Coll. Surf. A Physicochem. Eng. Asp. 624 (2021), 126766, https://doi.org/10.1016/j.colsurfa.2021.126766.

[38] R.M. Langford, M. Rogers, In situ lift-out: steps to improve yield and a comparison with other FIB TEM sample preparation techniques, Micron 39 (2008) 1325–1330, https://doi.org/10.1016/j.micron.2008.02.006.

[39] J.-P. Gatellier, J.-R. Disnar, Kinetics and mechanism of the reduction of Au(III) to Au(0) by sedimentary organic materials, Org. Geochem. 16 (1990) 631–640, https://doi.org/10.1016/0146-6380(90)90076-C.

[40] N.T.K. Thanh, N. Maclean, S. Mahiddine, Mechanisms of nucleation and growth of nanoparticles in solution, Chem. Rev. 114 (2014) 7610–7630, https://doi.org/10.1021/cr400544s.

[41] W. Di Cianni, M. de la Mata, F.J. Delgado, G. Desiderio, S.I. Molina, A.S. de León, M. Giocondo, Additive manufacturing of gold nanostructures using nonlinear photoreduction under controlled ionic diffusion, Int. J. Mol. Sci. 22 (2021) 7465, https://doi.org/10.3390/ijms22147465.

[42] Q. Tao, G. Pinter, T. Krivec, Influence of cooling rate and annealing on the DSC Tg of an epoxy resin, Microelectron. Reliab. 78 (2017) 396–400, https://doi.org/10.1016/j.microrel.2017.07.088.

[43] T. Mori, T. Hegmann, Determining the composition of gold nanoparticles: a compilation of shapes, sizes, and calculations using geometric considerations, J. Nanoparticle Res. 18 (2016) 295, https://doi.org/10.1007/s11051-016-3587-7.

[44] L.M. Liz-Marzán, C.R. Kagan, J.E. Millstone, Reproducibility in nanocrystal synthesis? Watch out for impurities, ACS Nano 14 (2020) 6359–6361, https://doi.org/10.1021/acsnano.0c04709.

[45] I. Roppolo, A. Doriguzzi Bozzo, M. Castellino, A. Chiappone, D. Perrone, K. Bejtka, S. Bocchini, M. Sangermano, A. Chiolerio, Dual step irradiation process for in situ generation and patterning of silver nanoparticles in a photocured film, RSC Adv. 6 (2016) 14832–14843, https://doi.org/10.1039/C5RA24234G.

[46] E. Fantino, A. Chiappone, I. Roppolo, D. Manfredi, R. Bongiovanni, C.F. Pirri, F. Calignano, 3D printing of conductive complex structures with in situ generation of silver nanoparticles, Adv. Mater. 28 (2016) 3712–3717, https://doi.org/10.1002/adma.201505109.

[47] G. Emanuele Lio, A. De Luca, C.P. Umeton, R. Caputo, Opto-mechanically induced thermoplasmonic response of unclonable flexible tags with hotspot fingerprint, J. Appl. Phys. 128 (2020), 93107, https://doi.org/10.1063/5.0018992.

[48] S. Bruzzone, M. Malvaldi, G.P. Arrighini, C. Guidotti, Light scattering by gold nanoparticles: role of simple dielectric models, J. Phys. Chem. B 108 (2004) 10853–10858, https://doi.org/10.1021/jp049401h.

[49] S.J. Oldenburg, Light Scattering from Gold Nanoshells, Diss. Rice University, 2000. https://scholarship.rice.edu/handle/1911/19543.

[50] M. Reynoso, I. Gauli, P. Measor, Refractive index and dispersion of transparent 3D printing photoresins, Opt. Mater. Express 11 (2021) 3392–3397, https://doi.org/10.1364/OME.438040.